Journal of Power Sources 194 (2009) 93–103

Contents lists available at ScienceDirect

Journal of Power Sources

journal homepage: www.elsevier.com/locate/jpowsour

Structural and electrical properties of magnetron sputtered Ti(ON) thin films: The case of TiN doped *in situ* with oxygen

A. Trenczek-Zajac[a,*], M. Radecka[a], K. Zakrzewska[b,1], A. Brudnik[b], E. Kusior[b], S. Bourgeois[c], M.C. Marco de Lucas[c], L. Imhoff[c]

[a] *Faculty of Materials Science and Ceramics, AGH University of Science and Technology, al. Mickiewicza 30, 30-059 Cracow, Poland*
[b] *Faculty of Electrical Engineering, Automatics, Computer Science and Electronics, AGH University of Science and Technology, al. Mickiewicza 30, 30-059 Cracow, Poland*
[c] *Institut Carnot de Bourgogne, UMR 5209 CNRS, Université de Bourgogne, 9 Avenue Alain Savary, BP 47870, 21078 Dijon cedex, France*

ARTICLE INFO

Article history:
Received 18 October 2008
Received in revised form 17 December 2008
Accepted 23 December 2008
Available online 3 January 2009

Keywords:
Titanium oxynitride
Magnetron sputtering
Thin films
Oxygen doping
Optical properties

ABSTRACT

Incorporation of oxygen into TiN lattice results in formation of titanium oxynitrides, TiO_xN_y that have become particularly interesting for photocatalytic applications. Elaboration as well as characterization of TiN and *in situ* oxygen-doped thin films is the subject of this paper. Thin films, 250–320 nm in thickness, have been deposited by dc-pulsed magnetron reactive sputtering from Ti target under controllable gas flows of Ar, N_2 and O_2. Optical monitoring of Ti plasma emission line at $\lambda = 500$ nm has been implemented in order to stabilize the sputtering rate. Scanning electron microscopy (SEM), X-ray diffraction in grazing incidence (GIXRD), micro-Raman spectroscopy, X-ray photoelectron spectroscopy (XPS), optical spectrophotometry and four-point probe electrical resistivity measurements have been performed in order to follow evolution of film physical parameters as a function of the oxygen flow rate η_{O_2} at which the films were deposited. The relationship between η_{O_2} expressed in standard cubic centimetres per minute, sccm and the nitrogen/oxygen content in thin films has been established by means of the analysis of the XPS spectra. GIXRD studies indicate that incorporation of oxygen results in a progressive loss of preferential orientation in ⟨1 1 1⟩ direction, a change in the grain size from 16 nm for TiN to about 3 nm for films deposited at $\eta_{O_2} = 1.32$ sccm and a decrease in the lattice constant. A systematic shift of all X-ray diffraction (XRD) lines towards higher diffraction angles is consistent with substitution of oxygen for nitrogen. Micro-Raman investigations indicate amorphisation of thin films upon oxidation. Binding energies determined from fitting of the XPS results concerning the N1s and Ti2p lines give evidence of the presence of TiO_xN_y compound. Red-shift of the plasma reflectance edge upon TiN oxidation is correlated with a decreased carrier concentration. Metal–semiconductor transition can be expected on the basis of the electrical conductivity decrease and development of the fundamental absorption across the forbidden band of TiO_2 upon increase in the oxygen flow rate. Additional absorption feature in the visible range, being a consequence of coexistence of free-electron and interband absorption within almost the same spectral range ($\lambda = 400$–600 nm) seems to be very promising for photocatalytic applications of titanium oxynitride thin films.

1. Introduction

Photocatalysis can be thought of as a potential solution to many problems related to pollution and contamination of air, water and soil, which have become a major concern of the modern society with its increasing ecological consciousness. Photoassisted processes are environmentally friendly in such a sense that they are based on the natural resources like solar radiation reaching the Earth, and as a consequence, H_2O and CO_2 are released into the atmosphere. These processes require an appropriate semiconductor to be used and titanium dioxide, in spite of its drawbacks, has been recognized as the most promising candidate for this purpose [1].

Conversion of solar energy into the chemical energy [2] is initiated by a photon absorption in a semiconductor. Upon absorption of the photon with an energy $h\nu$ equal or higher to the forbidden band gap energy E_g of the semiconductor, an electron–hole pair, e^-–h^+, is produced. Under conditions of negligible bulk and surface recombination, these charges can participate in redox reactions with contaminants adsorbed at the surface in the form of acceptors, A, or/and donors, D. These processes can be represented as follows:

$$\text{semiconductor} + h\nu \geq E \rightarrow h^+ + e^- \quad (1)$$

* Corresponding author. Tel.: +48 12 6172472; fax: +48 12 6172493.
E-mail address: anita_tr@agh.edu.pl (A. Trenczek-Zajac).
[1] Laboratoire Kastler-Brossel, Université P. et M. Curie, 4, place Jussieu, 75 005 Paris, France.

0378-7753/$ – see front matter © 2008 Elsevier B.V. All rights reserved.
doi:10.1016/j.jpowsour.2008.12.112

$$e^- + A \rightarrow A^{-\cdot} \quad (2)$$

$$h^+ + D \rightarrow D^{+\cdot} \quad (3)$$

where (2) represents reduction of acceptors and (3) corresponds to oxidation of donors.

Decomposition of many contaminants can be described by one of the reactions (2) or (3). The energy of the band gap E_g of the semiconductor, which assists in the creation of electron–hole pair, should be well-matched to the energy of the incident photons, i.e., $h\nu \geq E_g$. Too wide a band gap of TiO_2 (3.0 eV for rutile and 3.2 eV for anatase) constitutes a serious obstacle on the way to reach the appropriate efficiency of the photoconversion process within the visible range of the light spectrum.

In order to enhance the visible-light activity, some narrow-band semiconducting materials, e.g. GaAs (E_g = 1.4 eV) have been proposed [2] to substitute for otherwise the incontestable leader in the photocatalysis—TiO_2. However, they have failed to fulfil other basic requirements widely recognized for photo-processes. All conditions for an efficient photoactive semiconductor can be summarized [3,4] as follows:

(a) high stability and resistivity to corrosion and photocorrosion;
(b) low cost and availability;
(c) conduction band CB minimum and the dopant states above H_2/H_2O level;
(d) effective absorption of photons over the visible range, i.e., 1.6–2.5 eV;
(e) sufficient overlap between the intragap and band states of a photocatalyst in order to provide a fast transfer of photoexcited carriers to the reactive states at the surface within their lifetime.

Now, it is generally accepted that TiO_2 is the most promising material for photocatalytic applications as it meets almost all conditions. Biological and chemical inertness, resistance against corrosion, non-toxicity, high photo-oxidation potential, as well as a reasonable price [1–3] are its important advantages.

However, the practical exploitation of this semiconductor cannot be envisaged until a significant increase in the photocatalytic activity in the visible range has been reached. Many efforts have been undertaken to modify TiO_2 and mainly its absorption spectrum, while still preserving other properties important for photocatalysis. Majority of work has been directed toward metal ion doping, dye sensitization, incorporation of noble metals and formation of solid-solutions [2,4–10].

Since 2001, a series of papers has proclaimed a new generation of photocatalysts based on anion-doped TiO_2 [11–15]. Among those, the most important contribution came from Asahi et al. [11] who demonstrated that doping with non-metal atoms, such as carbon, sulphur, and nitrogen, resulted in a considerable shift of the fundamental absorption edge to the visible range (i.e., a red-shift). Since then, an avalanche of papers on the application of oxynitrides TiO_xN_y in photocatalysis has followed (see for example an excellent review in [3]). In some cases, an increase in the photo-conversion efficiency has been demonstrated but the reasons for the red-shift of the absorption spectrum of TiO_xN_y still remain unclear. Asahi et al. [11,12] originally attributed it to the band gap narrowing due to mixing of N2p states with O2p states forming the valence band of TiO_2. Later on, papers appeared that questioned the band gap narrowing in titanium oxynitrides [3]. Calculations based on spin-polarized density functional theory (DFT) performed by Di Valentin et al. [16] have led to a conclusion that N-doping causes no shift in position of both the edges of the valence and conduction bands as compared with undoped TiO_2. It was argued that incorporation of nitrogen resulted in an impurity band formation within the forbidden band gap of TiO_2. So far, no consensus on this problem has been reached and the scientific discussion is carried on [3]. However, it has been admitted that the red-shift of the absorption spectrum in TiO_xN_y is not always accompanied by an enhancement of the photoactivity.

Visible-light photoactivity of N-doped TiO_2 seems to be highly sensitive to the method of material elaboration, which, through its effect on the structure and morphology, affects the charge carriers mobility and has a strong influence on the recombination process. It is of paramount importance for photoactivated processes that the photoexited electron–hole pair recombination should be effectively limited or inhibited in order to allow the charge carriers to reach the metal–oxide surface where they participate in redox reactions. This creates a motivation for further development of the preparation methods of oxynitrides and especially those that allow for controllable deposition of thin films from constituents such as titanium, oxygen, and nitrogen.

Diversified approaches to the oxynitrides formation have been proposed. Modification of the existing structures consists in oxidation of TiN [15,17,18] or/and nitridation of TiO_2 either by thermal treatment in appropriate gas atmospheres or by direct implantation of nitrogen into TiO_2 [19]. It is also possible to build the oxynitrides from the precursors of TiN and TiO_2 in the chemical processes such a sol–gel technique or from mixing at the molecular level such as in the case of sputtering of Ti target in the controllable atmosphere of Ar, N_2 and O_2. This last method has been chosen by us in this work as it allows for the controllable change in the chemical composition and departure from stoichiometry [18,20].

Numerous papers have been published on deposition of thin films of nitrogen-doped TiO_2 or oxygen-doped TiN [21–27]. The most efficient methods of deposition seem to be LP-MOCVD (low-pressure metal organic chemical vacuum deposition) [21–24] and reactive magnetron sputtering [25,27].

In this work we have chosen direct incorporation of oxygen during growth of titanium nitride referred to as "*in situ* oxygen doping". Thin films were deposited by dc-pulse magnetron sputtering from Ti target under controllable gas flows of Ar, N_2 and O_2. The aim of this work was to demonstrate that this deposition method, when implemented with the optical control of the intensity of Ti emission line in the plasma and the stabilization of the gas flow rates, is suitable for oxynitrides formation. The influence of the technological parameters on the structural, morphological, electrical and optical properties of oxygen-doped TiN thin films was studied with the ultimate aim to improve their photoactivity towards the visible radiation. By increasing the oxygen flow rate at small intervals from $\eta_{O_2} = 0$ up to $\eta_{O_2} = 1.65$ sccm we wanted to get some insight into the mechanism of oxygen incorporation in TiN lattice. To the best of our knowledge, no such approach has been proposed. However, it should be mentioned that the initial stages of the oxidation of TiN and the kinetics of oxidation have been carefully studied in the past (see, for example [28]) in connection with intensively exploited applications of titanium nitride in microelectronics, particularly as diffusion barriers.

2. Experimental

2.1. Thin films preparation

Thin films were prepared in a planar, balanced, self-made magnetron sputtering system shown schematically in Fig. 1 and described in detail in [18,29]. A metallic Ti target of purity 99.95% was sputtered in reactive gas atmosphere containing Ar, N_2 and O_2. Argon, nitrogen and oxygen were introduced into the sputtering chamber individually, i.e., through separate gas admission lines. A closed-loop system with the optical control of plasma emission (optical emission spectroscopy—OES) was applied in order to stabilize the deposition rate in the intermediate region between

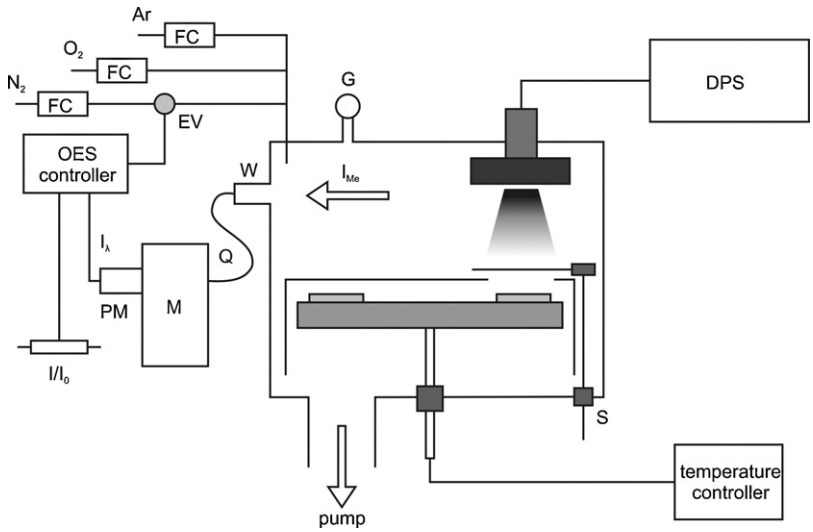

Fig. 1. Schematic view of the planar, self-made magnetron sputtering system used for elaboration of Ti–N–O thin films; FC, flow controller; OES, optical emission spectroscopy; EV, electromagnetic valve; PM, photomultiplier; M, monochromator; Q, optical fiber; W, transparent window; DPS, DC power supply; S, shutter; and G, pressure gauge.

two stable sputtering modes: reactive and metallic. The magnetron discharge was driven by a dc-pulse power supply (Dora Power System—DSP) the details of which are given in [30]. The substrate holder was at the ground potential, no bias was applied, the cathode current was stabilized at 2 A, the power for each deposition run was maintained at 0.9 kW.

The applied optical control system is based on continuous monitoring of intensity I_{Me} of a chosen plasma emission line being a result of de-excitation of metal species present during sputtering. Light extracted from the plasma ring, formed below the sputtered target, is transmitted via an optical fiber to the SPM2 Zeiss monochromator as shown in Fig. 1. The emitted light is collected from the region of about 5 mm below the target, while the target-to-substrate distance is 35 mm. The intensity of light at a given wavelength, I_λ, detected by a photomultiplier, serves as a feedback signal for admission of the reactive gas in the flow regulation system (for detailed description see [29]).

For deposition of nitrides and oxides of titanium, the relative ratio of the intensity I/I_0 of Ti emission line at $\lambda = 500$ nm is used as an important technological parameter. The I_0 corresponds to the intensity of the same emission line for deposition of Ti at 100% Ar, i.e., in a pure metallic mode. The intensity ratio I/I_0 is the parameter that controls the sputtering rate through its influence on the state of target poisoning. The I/I_0 is an indirect measure of the flux of titanium species arriving at the substrate. In general, low value of I/I_0 indicates low sputtering rate of Ti target either in nitrogen- or in oxygen-rich atmosphere.

Using such a system, both oxygen-doped titanium nitride and nitrogen-doped titanium dioxide can be obtained. This was demonstrated in our previous paper [31]. Here, we have concentrated upon elaboration of oxygen-doped titanium nitride thin films starting from the conditions as close as possible to those for stoichiometric TiN deposition, i.e., $I/I_0 = 0.5$. It has indeed been established previously [18] that $I/I_0 = 0.5$ leads to stoichiometric TiN.

In the particular case of oxygen-doped titanium nitride, for all deposited samples $I/I_0 = 0.5$ was kept constant by dynamic modification in nitrogen flow rate η_{N_2} in the feedback regulation system provided by OES (see Table 1). For a given deposition run, gas flows of argon η_{Ar} and oxygen η_{O_2} were set up at constant values by MKS gas flow controllers. The films with different nitrogen/oxygen ratios incorporated were obtained at consecutive deposition runs, which differed by oxygen flow rates η_{O_2}.

To provide good thickness homogeneity and film crystallinity, a rotating substrate holder equipped with a resistive heater was used. Thin films of thicknesses between 250 nm and 320 nm were deposited at elevated temperature of about 250 °C. Film thickness was measured mechanically with the help of a Talysurf profilometer.

Different substrates: Corning glass, amorphous silica and silicon wafers were applied depending on the subsequent measurements to be performed.

2.2. Characterisation methods

2.2.1. Morphology analysis

Both, surface and cross-sectional morphology of thin films were studied by means of scanning electron microscopy (SEM). Thin films for this purpose were deposited mostly onto amorphous silica and metalized before analysis. Measurements were performed on a JEOL JSM 6400F instrument, working typically at 15 keV.

Table 1
Ti(ON) thin film parameters: thickness, lattice constant, grain size as a function of the oxygen flow rate.

Oxygen flow rate, η_{O_2} (sccm)	Average nitrogen flow rate, η_{N_2} (sccm)	Films thickness, d (nm)	Lattice parameter, a (nm)	Grain size from XRD (nm)
0	1.30	250	0.424	16.1
0.46	0.96	255	0.423	16.2
0.66	0.82	265	0.418	15.4
0.86	0.80	315	0.417	12.2
0.99	0.66	280	0.417	7.8
1.32	0.45	270	0.416	2.8
1.65	0.30	280	–	–

Thin films were deposited by dc-pulse reactive magnetron sputtering at total pressure 1 Pa, argon flow rate $\eta_{Ar} = 8$ sccm, magnetron current 2 A; power 0.9 kW, substrate temperature $T_s = 250$ °C, $I/I_0 = 0.5$.

2.2.2. Structural analysis

The structural characterization of thin films was carried out by means of X-ray diffraction at grazing incidence (GID) configuration. A Philips X'Pert MPD diffractometer with Cu Kα filtered radiation was used over the 2θ range from 15° to 80°. Phase identification was performed using the ICDD database. Lattice parameter was obtained by means of a Rietveld refinement. The average grain size was estimated from the well-known Scherrer formula [32] after taking into account the instrumental broadening. As a complementary method, the micro-Raman spectroscopy was employed. Raman spectra were obtained with a Jobin-Yvon T64000 spectrometer. A nitrogen-cooled CCD was used as detector. The excitation was provided by an Ar–Kr ion laser and the spectra were recorded in a back-scattering configuration. The wavelength was 514 nm and the excitation power was kept low enough to avoid heating of the samples. Thin films for structural analysis were deposited onto amorphous silica.

2.2.3. XPS measurements and analysis

The measurements were performed with a SIA 100 Riber system. An Al Kα X-ray source (energy of 1486.6 eV) was used with 300 W power (accelerating voltage 12 kV and emission current 25 mA). A MAC 2 Riber spectrometer was used for photoelectron analysis with its axis in the direction perpendicular to the surface of the sample. Total resolutions including primary photons and spectrometer, as derived from the linewidth of Ag $3d_{5/2}$, were equal to 2.0 eV for global spectra and to 1.3 eV for windows corresponding to the selected lines. The Casa software package was used for data treatments such as a background subtraction with a Shirley routine, multiple components fittings of the spectra and peak area calculations. Contributions of Gauss (60%) and Lorentz (40%) functions were taken into account for desummation of complex peaks. The calibration of binding energy axis was based on C1s line at 284.5 eV. As verified by Ar^+ bombardment, carbon can be considered as an adsorbed contamination. Ar^+ sputtering was performed at an incident angle of 60°. In the quantitative analysis the peak areas were corrected taking into account the different photoionization cross-sections as well as energy dependence of both the spectrometer transmission and the electron mean free path.

2.2.4. Spectrophotometric studies

The optical transmittance and reflectance spectra were recorded at room temperature for samples deposited onto amorphous silica. A Lambda 19 Perkin–Elmer double beam spectrophotometer equipped with a 150 mm integrating sphere was used to measure the spectral dependence of the diffuse reflectance and transmittance over a wide range of wavelengths, λ, from 250 nm to 2200 nm.

2.2.5. Electrical measurements

DC electrical resistance at room temperature was measured by means of a four-probe method. It was verified that the $U(I)$ measurements performed over the range 0.001–0.229 mA for the applied current, I, and 0.001–1.416 V for the resulting voltage drop, U, gave the results well within the applicability of the Ohm's law. Electrical sheet resistance, i.e., the resistance of the square area R_{sq} was calculated. Given the film thickness, d, the bulk conductivity σ could be found from:

$$\sigma = \frac{1}{R_{sq} d} \tag{4}$$

3. Results and discussion

Typical examples of the cross-sectional and surface SEM images of TiN and oxygen-doped Ti(ON) thin films deposited by dc-magnetron sputtering are shown in Fig. 2. The cross-sectional images reveal columnar growth of TiN thin films (Fig. 2a). The columnar mode of growth remains in agreement with the Thornton model [33] because the substrate temperature 250 °C during the film deposition is much smaller than the melting point of TiN. For TiN thin films doped with oxygen (Fig. 2b) the growth of columns is perturbed. SEM surface images (Fig. 2c and d) indicate that the film surface is very smooth.

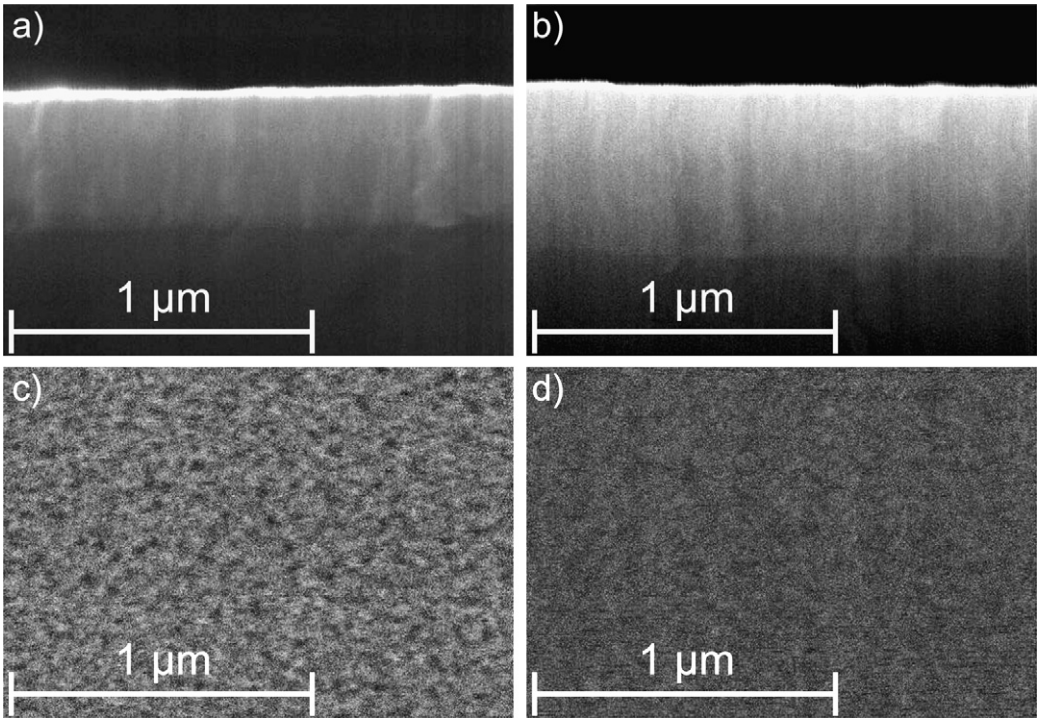

Fig. 2. Scanning electron microscope (SEM) images of TiN and oxygen-doped thin films deposited by reactive magnetron sputtering onto silicon wafers; cross-sections (a, b) and surfaces (c, d) of TiN (a, c) and Ti(ON), oxygen flow $\eta_{O_2} = 1.32$ sccm (b, d).

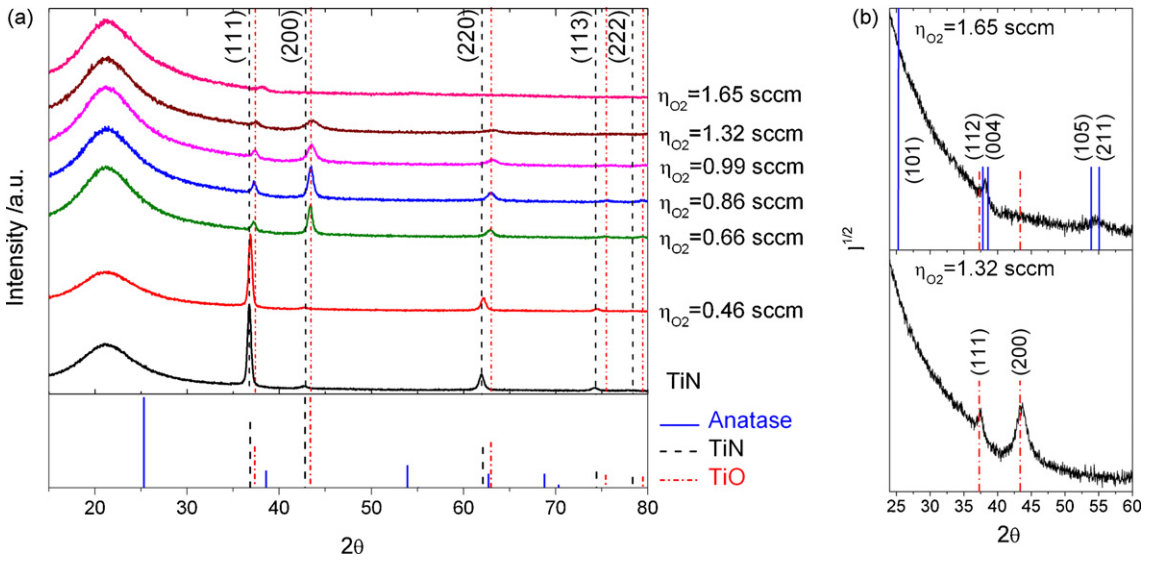

Fig. 3. X-ray diffraction patterns in GID configuration of TiN and oxygen-doped Ti(ON) thin films deposited by reactive magnetron sputtering onto amorphous silica at different oxygen flow rates. Vertical lines mark peak positions according to ICDD database: solid, anatase; dashed, TiN; dashed-dotted, TiO.

X-ray diffraction patterns recorded in GID configuration are presented in Fig. 3 while the results of analysis are included in Table 1. As one can see, the titanium nitride film ($\eta_{O_2} = 0$) as well as the film obtained at the lowest oxygen flow rate ($\eta_{O_2} = 0.46$ sccm) display almost the same diffraction pattern corresponding to a well-crystallized structure isomorphic to fcc cubic TiN. Moreover, these films show a preferential orientation in the ⟨1 1 1⟩ direction. In a typical, non-oriented TiN the intensity ratio of $I(1\,1\,1)/I(0\,0\,2)$ is 0.66 [34]. It can be inferred from XRD diffraction pattern for TiN presented in Fig. 3a that $I(1\,1\,1)/I(0\,0\,2)$ amounts to about 10. Thermodynamic conditions during the deposition process are responsible for this mode of growth, which has been reported previously for TiN films fabricated by reactive sputtering [35].

The increase in the oxygen flow rate above 0.5 sccm induces significant changes in the XRD pattern. The ratio of $I(1\,1\,1)/I(0\,0\,2)$ drops below 1, indicating disappearance of the preferential orientation in ⟨1 1 1⟩ direction followed by the substantial loss in film crystallinity. As shown in Table 1, the grain size decreases with the increasing oxygen flow rate. This is consistent with a substantial broadening of all diffraction peaks.

As one can see in Fig. 3a, doping with oxygen results in a systematic shift of all peaks towards higher diffraction angles with respect to the angular positions typical for TiN. This corresponds to a decrease in the lattice constant a from $a = 0.424$ nm at $\eta_{O_2} = 0$ to $a = 0.416$ nm at $\eta_{O_2} = 1.32$ sccm, as shown in Table 1. As the atomic radius of oxygen is smaller than that of nitrogen [36], this effect can be accounted for by substitution of oxygen for nitrogen. Similar behaviour has been reported [37] and attributed to titanium oxynitride formation.

However, at the highest oxygen flow rates $\eta_{O_2} = 1.32$ sccm and $\eta_{O_2} = 1.65$ sccm, the intensity of XRD peaks is quite small and their width is increased indicating substantial amorphisation. Loss of crystallinity with an increased concentration of oxygen has been observed by Vaz et al. [27] in TiN_xO_y thin films prepared by magnetron sputtering. Oxygen is much more reactive than nitrogen and its excess leads to supersaturation effect that puts constrains on crystallisation of TiN.

Based on XRD results, one can assume that at $\eta_{O_2} > 0.5$ sccm the solid solution of TiN with the lower oxide phase of titanium, TiO is formed. Both TiN and TiO crystallize in the same crystallographic structure (cubic) and have similar lattice parameters ($a_{TiN} = 0.42417$ nm [38] and $a_{TiO} = 0.41770$ nm [39]). The systematic shift in the angular peak position with the increased η_{O_2} is in favour of this interpretation. In fact, formation of TiN–TiO solid solution, equivalent to titanium oxynitride, TiN_xO_y, over the range of oxygen flow rate η_{O_2} from 0.5 sccm to 1.32 sccm is indicated by the values of lattice constant (Table 1).

However, at the highest oxygen flow rates $\eta_{O_2} = 1.65$ sccm one can notice (Fig. 3b) the onset of precipitation of very weakly crystallized anatase in the amorphous background. The X-ray diffraction patterns of samples obtained at $\eta_{O_2} = 1.32$ sccm and $\eta_{O_2} = 1.65$ sccm are poorly developed but differ substantially. At the oxygen flow of 1.65 sccm, only two wide and small peaks can be seen while TiO (2 0 0) peak present at $\eta_{O_2} = 1.32$ sccm disappears. The remaining two peaks have been identified: at $\theta = 38.2$ as (0 0 4) and (1 1 2) while at $\theta = 54.6$ as (1 0 5) and (2 1 1) reflections of anatase TiO_2.

At the highest η_{O_2} one can expect the excess of oxygen that cannot be accommodated in TiN_xO_y hence the precipitation of TiO_2 begins.

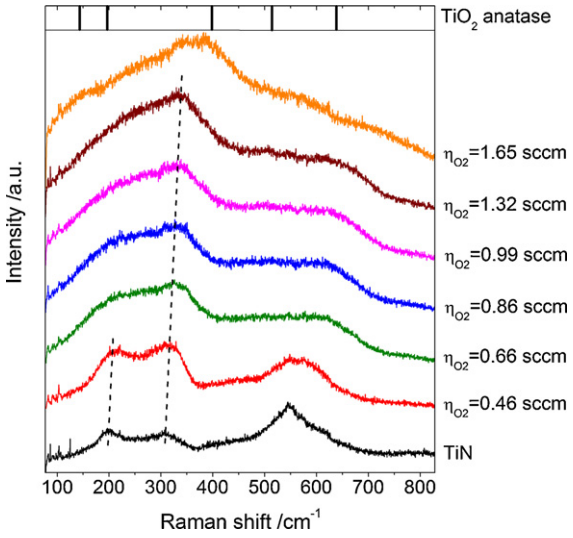

Fig. 4. Raman spectra of TiN and oxygen-doped Ti(ON) thin films deposited by reactive magnetron sputtering onto amorphous silica at different oxygen flow rates η_{O_2}. Peak positions for TiO_2 anatase are indicated at the top.

The structure of deposited thin films was further studied by micro-Raman spectroscopy. This method is not only complementary to the XRD technique but also sensitive to the presence of amorphous phase. The Raman spectra of thin films grown on amorphous silica substrates are presented in Fig. 4.

Titanium nitride with its Fm3m crystallographic symmetry has no first order Raman-active vibrations and thus, only disorder-allowed modes and second order scattering can be observed. The low-frequency scattering below 370 cm^{-1} is caused by acoustic phonons [40]. The high-frequency scattering around 560 cm^{-1} is due to optical phonons together with the second-order contributions combining acoustic and optical modes. Sprengler et al. [40] showed that the second-order scattering is predominant in stoichiometric TiN, while first-order Raman scattering increases with increasing nitrogen deficiency.

The spectrum of the film obtained $\eta_{O_2} = 0$ (Fig. 4) indicates the growth of almost stoichiometric TiN. The introduction of a small flow of oxygen ($\eta_{O_2} = 0.46$ sccm) during the deposition process leads to small but significant changes in the Raman spectrum: an increase in the relative intensity of the acoustic bands and a shift to higher frequencies of the first peak of the Raman scattering over the acoustic range. Sprengler et al. [40] related this shift to the deviation

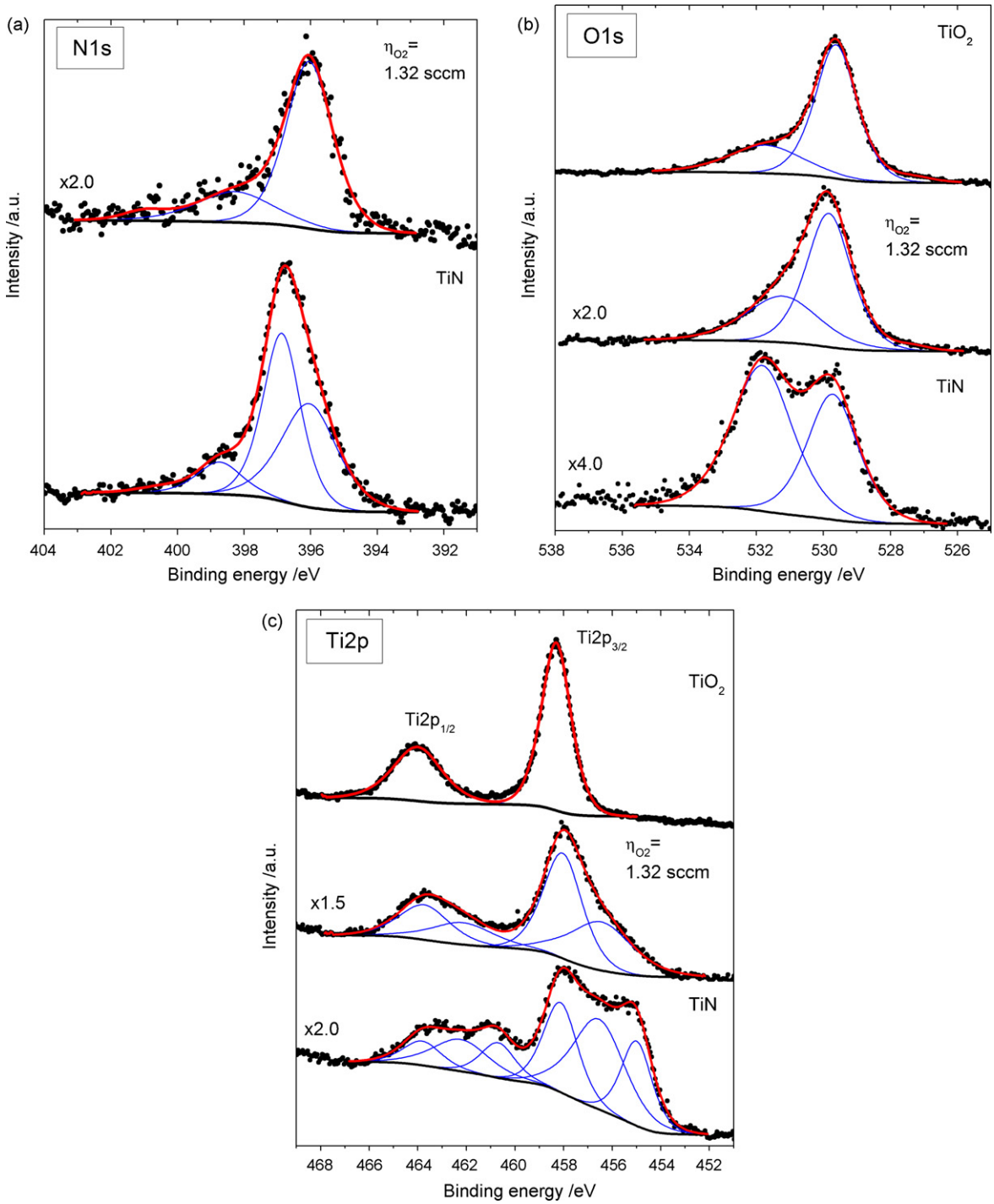

Fig. 5. XPS results for TiN and Ti(ON), thin films deposited by reactive magnetron sputtering at different oxygen flow rates η_{O_2} (a) N1s (b) O1s, and (c) Ti2p.

from TiN stoichiometry. In this case, a shift by about 10 cm^{-1} of the first Raman peak indicates a small deviation from stoichiometry, lower than 3%.

The increase in the oxygen flow rate η_{O_2} over the 0.5–1.32 sccm range leads to a significant broadening of the Raman bands. At the same time, the maximum of the acoustic band at about 310 cm^{-1} shifts systematically to higher frequencies. These effects in the Raman spectrum correlate well with those in the XRD patterns indicating a progressive amorphisation of the films and the disappearance of the preferential orientation in the ⟨1 1 1⟩ direction.

At the oxygen flow of $\eta_{O_2} = 1.65$ sccm, the shape of the Raman spectrum changes: new broad contributions begin to appear over the low-frequency range around 150 cm^{-1}, but also at 390 and 550–600 cm^{-1}. These new contributions can be interpreted as the first sign of the appearance of titanium dioxide largely in an amorphous phase [41]. The lines corresponding the Raman peak positions of well-crystallized anatase are given for comparison in Fig. 4.

XPS investigations bring a new insight into the problem of composition of thin films and thanks to possibility of determining the oxidation states of Ti and N they can help to answer the question whether it is possible to have TiO_2 along with TiN_xO_y in magnetron sputtered thin films. Such investigations have been conducted before [37] and have led to the conclusion that based on XPS results one can confirm formation of amorphous titanium dioxide.

XPS spectra corresponding to N1s, O1s and Ti2p lines are shown in Fig. 5 for TiN ($\eta_{O_2} = 0$) and a thin film deposited at $\eta_{O_2} =$ 1.32 sccm. XPS spectrum of stoichiometric TiO_2 deposited by means of the same technology, i.e., magnetron sputtering, is shown for comparison. All the binding energies determined from the fitting of the different lines are presented in Table 2.

Nitrogen N1s XPS spectra are presented in Fig. 5a. The shape of N1s peaks is complex for both cases: TiN and that of oxygen-doped films deposited at $\eta_{O_2} = 1.32$ sccm. The principal component of TiN N1s peak occurs at the binding energy of 396.9 eV and corresponds to chemical bonding Ti–N in the stoichiometric titanium nitride [42,43]. This component is missing in the case of oxygen-doped thin film ($\eta_{O_2} = 1.32$ sccm). However, in the case of TiN, in order to fit the experimental spectrum it is necessary to introduce two other components: one at 396.0 eV and another at 398.7 eV. Lower energy component at 396.0 eV can be assigned to O–Ti–N bonding [44–47] while higher energy component at 398.7 eV has been ascribed to chemisorbed molecular nitrogen [15,19,43,47–51].

For thin films obtained at $\eta_{O_2} = 1.32$ sccm, a reduction of intensity of the N1s peak by a factor of 2 as compared with that in TiN can be observed (Fig. 5a). The main contribution to this peak is now 396.0 eV with a secondary component at about 398.3 eV. Many authors postulate that the XPS peaks at binding energies (of about 396 eV) lower than that of Ti–N (397 eV) indicates that TiO_xN_y is formed [44–47]. On the contrary, the assignment of high-energy components of N1s peaks, appearing at binding energies 398 eV and higher, cannot be made unequivocally. From the literature data, these peaks could be related to chemisorbed molecular nitrogen or to fraction of N_2 released from oxidation of titanium nitride [15,19,45,47–51]. Therefore, the presence of component of N1s peak at 396.0 eV proves that TiN_xO_y is formed at the surface of deposited films. Even TiN thin film deposited by reactive magnetron sputtering at $\eta_{O_2} = 0$ is not free from this component.

XPS O1s peaks shown Fig. 5b confirm that even in the case of apparently undoped TiN, the film is partially oxidized, certainly at the surface. O1s peak has low intensity in this case but is composed of two peaks of almost the same height, located at 529.7 eV and 531.8 eV. These two peaks are also observed in oxygen-doped thin films ($\eta_{O_2} = 1.32$ sccm) and TiO_2. For oxygen-doped thin films obtained at $\eta_{O_2} = 1.32$ sccm the intensity of the component at 529.7 eV increases considerably as compared with the corresponding contribution in TiN, while the second peak at 531.8 eV does not change so much. For TiO_2, the ratio of intensities of these two components remain the same as in the case of the film obtained at $\eta_{O_2} = 1.32$ sccm. The lower-energy component of O1s XPS peak at about 529.6–529.8 eV could be assigned to lattice oxygen of the same coordination to titanium as in TiO_2 while higher-energy component at 531.2–531.7 eV corresponds to oxygen adsorbed at the surface [43,52].

The most important difference can be seen in Ti2p XPS spectra for undoped TiN, oxygen-doped thin films deposited at $\eta_{O_2} =$ 1.32 sccm and TiO_2 (Fig. 5c). The Ti2p peaks for TiO_2 and that for thin films doped with oxygen ($\eta_{O_2} = 1.32$ sccm) are clearly dominated by the characteristic doublet $2p_{3/2}$ at 458.3 eV and $2p_{1/2}$ at 464.0 eV.

Ti2p line is far more complex in the case of undoped TiN as three contributions of almost equal intensities are necessary to fit

Table 2
N1s, O1s and Ti2p characteristic binding energies as determined from XPS results for different thin films: TiN, Ti(ON) deposited at oxygen flow $\eta_{O_2} = 1.32$ sccm and TiO_2.

Sample	Binding energy (eV)	Bonding	
		Type	Literature
N1s			
TiN	396.0	O–Ti–N	[44–47]
	396.9	Ti–N bonding in TiN	[42,43]
	398.7	Chemisorbed molecular nitrogen or fraction of N_2 released from oxidation of titanium nitride	[15,19,45,47–51]
Ti(ON) $\eta_{O_2} = 1.32$ sccm	396.0	O–Ti–N	[44–47]
	398.3	Chemisorbed molecular nitrogen or fraction of N_2 released from oxidation of titanium nitride	[15,19,45,47–51]
O1s			
TiN	529.7	Ti–O–Ti-like in TiO_2	[43]
	531.8	Chemisorbed O_2	[52]
Ti(ON) $\eta_{O_2} = 1.32$ sccm	529.8	Ti–O–Ti-like in TiO_2	[43]
	531.2	Chemisorbed O_2	[52]
TiO_2	529.6	Ti–O–Ti-like in TiO_2	[43]
	531.7	Chemisorbed O_2	[52]
$Ti2p_{3/2}$			
TiN	455.0	$Ti2p_{3/2}$, Ti–N in TiN	[56]
	456.6	N–Ti–N or O–Ti–N in TiO_2:N	[56]
	458.1	$Ti2p_{3/2}$, O-Ti-O like in TiO_2, loss peak	[52,53,57]
Ti(ON) $\eta_{O_2} = 1.32$ sccm	456.5	N–Ti–N or O–Ti–N in TiO_2:N	[56]
	458.1	$Ti2p_{3/2}$, O–Ti–O like in TiO_2, loss peak	[52,53,57]
TiO_2	458.2	$Ti2p_{3/2}$, O–Ti–O like in TiO_2	[52,53]

the spectrum. By comparison with the binding energies available in the literature [52,53], contributions of TiO_2 and TiN are clearly evidenced with respective $Ti2p_{3/2}$ binding energies at 458.1 eV and 455.0 eV, respectively (see Table 2). It was indeed demonstrated that exposure to air or oxygen atmosphere causes a surface oxidation of TiN [54]. In addition, an intermediate $Ti2p_{3/2}$ component at 456.6 eV has to be taken into account (see Table 2). This intermediate component could be assigned to titanium oxynitride [52,55]. It is interesting to note that this kind of chemical environment of Ti with O and N is present in all the studied samples, except for TiO_2, but with different relative intensities.

The presence of XPS components corresponding to TiO_2 in all the samples even in TiN can be well accounted for by oxidation of the surface being a result of air exposure before XPS analyses. However, the presence of titanium oxynitride species is well evidenced in XPS results: with oxygen added during the film growth, substitution of nitrogen by oxygen occurs leading to another kind of bonding of titanium species which could have important influence on thin films properties.

As the depth of XPS analysis is limited to about 10 nm outermost layer one may argue that the presence of TiO_2 occurs at the film surface, only. In order not to be only surface sensitive, XPS experiments were also performed after Ar+ bombardments leading to the sputtering of the surface layer. After sputtering, Ti2p lines of thin films doped with oxygen ($\eta_{O_2} = 1.32$ sccm) can be decomposed introducing the special shape [24] characteristic of sputtered titanium dioxide (with the maximum of the $Ti2p_{3/2}$ line at 458.1 eV) thus evidencing the presence of TiO_2 species in titanium oxynitride.

In addition, in order to get information on the relative contributions of oxygen and nitrogen in the films, quantifications were performed using O1s, N1s and Ti2p peak area.

The evolutions of nitrogen/titanium as well as that of oxygen/titanium calculated from XPS results as functions of the oxygen flow rate are shown in Fig. 6. As expected the N/Ti ratio decreases while O/Ti increases with the increased oxygen flow rate η_{O_2}. In the

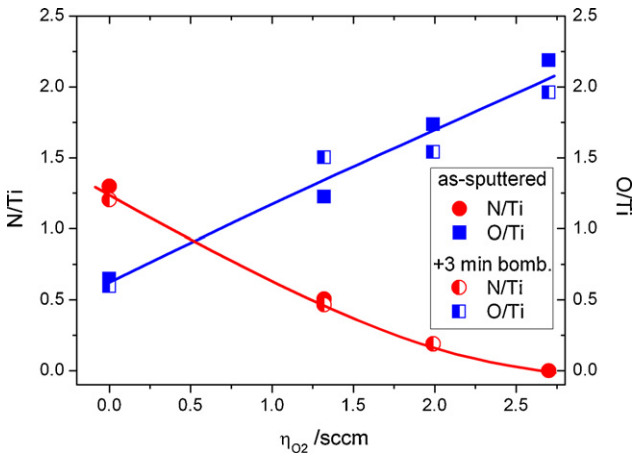

Fig. 6. Atomic ratio of N/Ti and O/Ti in thin films as a function of the oxygen flow rate η_{O_2}.

case of TiN ($\eta_{O_2} = 0$), N/Ti is slightly greater than 1 which indicates an over-stoichiometry but O/Ti is more than 0.5. One can observe that such an excess of oxygen is present not only at the film surface but also in the bulk, as confirmed by the studies after Ar^+ bombardment. The excess of oxygen remains at all oxygen flow rates applied in this work.

This effect was previously reported from XPS analysis of oxynitrides thin films [24,37] and attribute to the coexistence of TiO_xN_y with TiO_2.

Optical reflectance $R(\lambda)$ and transmittance $T(\lambda)$ spectra of TiN and Ti(ON) thin films deposited onto transparent, amorphous silica substrates are presented in Fig. 7a and b, respectively.

The characteristic feature of the reflectance spectra $R(\lambda)$ of the TiN and the films deposited at low oxygen flow rates is a distinct minimum (Fig. 7a) that occurs in the visible region within the

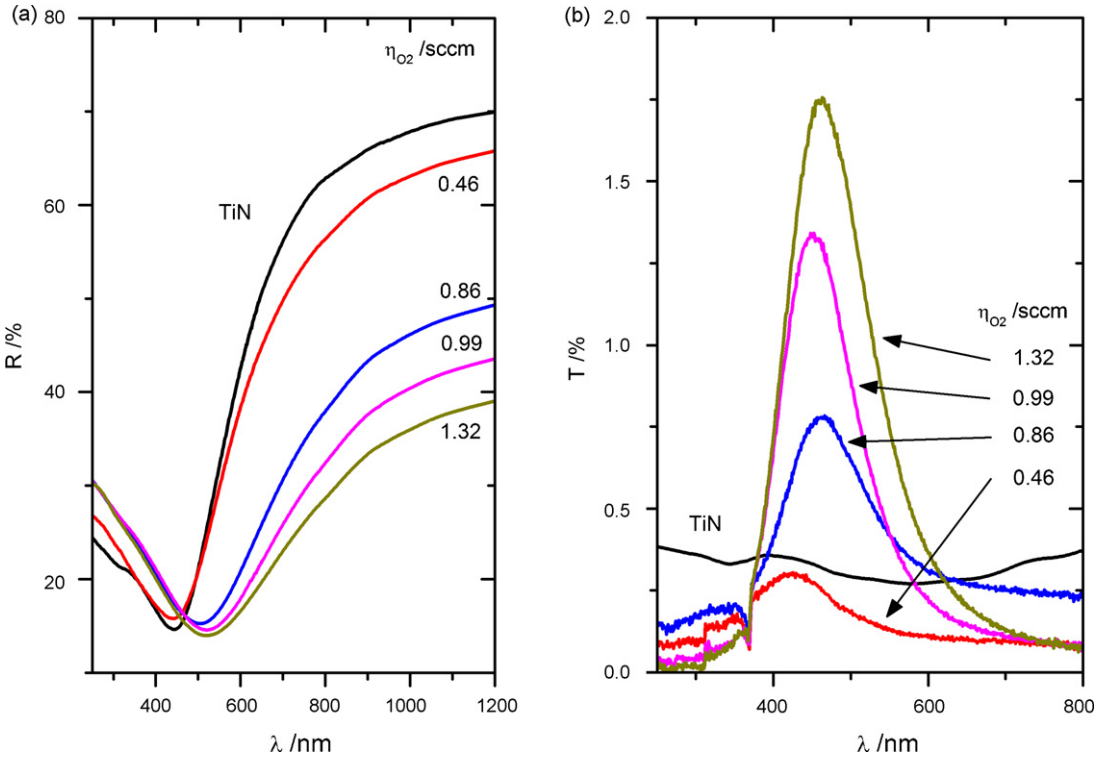

Fig. 7. Optical coefficient of (a) reflectance $R(\lambda)$ and (b) ransmittance $T(\lambda)$ as a function of wavelength λ for TiN and oxygen-doped Ti(ON) thin films deposited onto amorphous silica at different oxygen flow rates η_{O_2}.

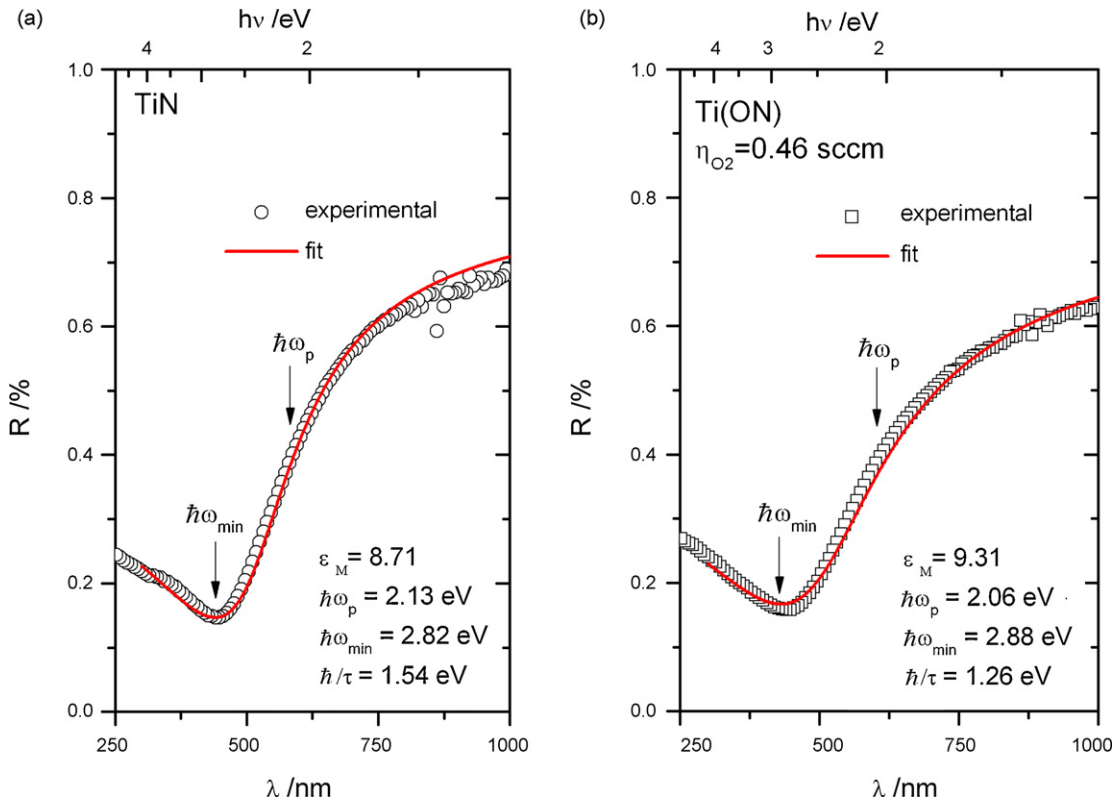

Fig. 8. Fit of Drude model to the experimental data of the optical reflectance $R(\lambda)$ for TiN and oxygen-doped Ti(ON) deposited at $\eta_{O_2} = 0.46$ sccm.

range of wavelengths $\lambda = 400–600$ nm followed by an abrupt rise in the reflectance coefficient for longer wavelengths. This so-called plasma reflectance edge is typical for materials with light absorption by a free-electron gas and can be accounted for by Drude model [58].

Pure stoichiometric TiN exhibits metallic character and its gold-like tint in the reflected light corresponds well with the occurrence of the plasma reflectance edge in the visible range of the light spectrum. Oxygen-doped thin films obtained in this work retain up to $\eta_{O_2} = 1.32$ sccm the most important properties of the reflectance characteristics of pure TiN. Nevertheless, it should be noted (Fig. 7a) that there is a pronounced red-shift position of reflectance minimum with an increasing oxygen doping and that the plasma reflectance edge is less steep at long wavelength limit. The reflectance does not reach such high values (40–50%, only) as in the case of TiN (70%).

The most significant differences between oxygen-doped and pure TiN manifest themselves in the optical transmission $T(\lambda)$ (Fig. 7b). Stoichiometric TiN is almost opaque and its transmittance coefficient (of about 0.3–0.4%) does not show any remarkable dependence on wavelength. However, even the smallest amount of oxygen incorporated in TiN affects the transmission spectrum in such a way that a maximum in $T(\lambda)$ appears. Upon the increasing oxygen flow rate, this maximum becomes more important (up to 1.8% at $\eta_{O_2} = 1.32$ sccm) and its position moves towards longer wavelengths. The reasons for this particular behaviour of transmission should be sought for in two different mechanisms of light absorption: the first one – free-electron absorption and another one is the fundamental interband absorption typical for semiconductors such as TiO_2. These two mechanisms, normally well-separated, take place almost in the same spectral range, probably because of the oxynitrides formation.

For oxygen-doped TiN, the free-carrier absorption is responsible for the decrease in the optical transmittance at wavelengths longer than 500 nm. A substantial decrease in the optical transmittance with a decreased wavelengths below 500 nm is a result of the fundamental absorption of photons with the energy comparable to the separation between the valence and conduction band E_g as in TiO_2. The onset of fundamental absorption edge could be detected even at the lowest oxygen flow rate ($\eta_{O_2} = 0.46$ sccm). This effect is of paramount importance from the point of view of photocatalytical applications. The increased absorption in the visible range of the light spectrum offers much promise for the enhancement of the photocatalytic efficiency in the photodegradation processes.

According to the theory of light absorption on free carries, there is correlation between the value of plasma frequency ω_p, the frequency ω_{min} at which the minimum in the reflectance coefficient occurs and the carrier concentration, N.

In the classical free-electron theory (Drude model), the real ε' and imaginary ε'' part of the dielectric constant are expressed as

$$\varepsilon' = \varepsilon_M - \frac{\omega_N^2}{\omega^2 + 1/\tau^2} \quad \text{and} \quad \varepsilon'' = \frac{1}{\omega\tau}\frac{\omega_N^2}{\omega^2 + 1/\tau^2} \tag{5}$$

where ω_N^2 stands for $4\pi Ne^2/m_{eff}$, m_{eff} is an effective mass, $1/\tau$ is a damping constant.

Based on ε' and ε'' the spectral dependence of the reflectance coefficient $R(\lambda)$ can be theoretically predicted and fitted to the experimental points. This was done and shown in Fig. 8.

The best fit of the Drude model requires the following parameters: high-frequency dielectric constant, ε_M, the plasma frequency ω_p and the damping constant $1/\tau$. The plasma frequency ω_p is a characteristic point at which $\varepsilon' = 0$. From this condition the plasma frequency can be found as

$$\omega_p = (4\pi Ne^2/\varepsilon_M m_{eff})^{1/2} \tag{6}$$

At $\varepsilon' = 0$, the electron gas undergoes volume plasma oscillations and at frequencies $\omega < \omega_p$, i.e., at wavelengths longer than the one

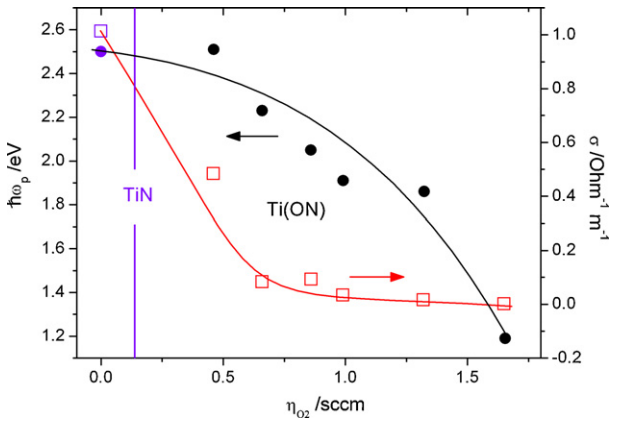

Fig. 9. Plasma frequency ω_p calculated from the fits of Drude model and measured conductivity σ as a function of oxygen flow η_{O_2}.

corresponding to plasma frequency $\lambda > \lambda_p$, high reflectance occurs [59]. For $\omega > \omega_p$ the reflectance decreases sharply but it reaches the minimum not at the plasma frequency ω_p but at ω_{min} (or λ_{min}) where $\varepsilon' = 1$ and $\varepsilon'' \ll 1$, i.e., the point at which the refractive index n approaches that of air [59]. The frequency at which the minimum in reflectance occurs is given by

$$\omega_{min} = (4\pi Ne^2/(\varepsilon_M - 1)m_{eff})^{1/2} \quad (7)$$

Variations of plasma frequency ω_p derived from the fit of Drude model to the experimental data should be linked to modifications in free electron concentration, N, according to Eq. (6). Thus, the decrease in ω_p observed upon increasing oxygen flow rate η_{O_2} which corresponds to a decrease in carrier concentration should be related to an increase in the electrical resistance of the films. This can be clearly seen in Fig. 9 where both the plasma frequency and the electrical conductivity are plotted as functions of oxygen flow rate. All these effects confirm oxidation of titanium nitride.

4. Conclusions

DC-pulse magnetron sputtering from Ti target in the reactive gas atmosphere being a mixture of argon, nitrogen and oxygen with a flow-rate controllable amount of each component was used to deposit TiN and *in situ* oxygen-doped Ti(ON) thin films. Implementation of a closed-loop system with the optical control of plasma emission (optical emission spectroscopy) allowed to stabilize the deposition rate within the intermediate region between two stable sputtering modes: reactive and metallic. This elaboration method turned out to be successful for following the evolution of changes in the morphology, microstructure and electronic parameters during the first stages of oxynitrides formation.

SEM images, both cross-section and surface revealed perturbation of columnar growth of TiN and surface smoothness upon an increase in the oxygen flow rate during deposition. This might be due to the partial amorphisation of TiN doped with oxygen confirmed by both X-ray diffraction data as well as by micro-Raman spectroscopy. Well-crystallized TiN thin films with the preferred crystallographic orientation in ⟨1 1 1⟩ direction and a grain size of about 16 nm gave way to randomly oriented polycrystalline Ti(ON) of smaller grain size when deposited at the intermediate oxygen flow rate. The micro-Raman spectra were sensitive to this evolution. X-ray diffraction patterns of TiN doped with oxygen were systematically shifted towards higher diffraction angles what indicated a decrease in the lattice constant and substitution of nitrogen by oxygen. For the highest oxygen flow rate, the changes in the XRD patterns and Raman spectra suggest the onset of precipitation of weakly developed anatase TiO_2 crystallites in the amorphous background. XPS investigations confirmed the growth of titanium oxynitride and the increase of the oxygen concentration in the films when increasing the oxygen flow rate, while the nitrogen quantity decreases. Optical measurements indicated the development of fundamental absorption edge, typical for semiconductors. Optical reflectance spectrum demonstrated a characteristic feature, the minimum followed by an abrupt increase at longer wavelength. This plasma reflectance edge is typical for free-electron absorption accounted for by the Drude model. Displacement of the plasma reflectance edge towards longer wavelengths (lower frequencies) upon TiN doping with oxygen could be attributed to the decreased concentration of charge carriers. Plasma frequency ω_p, one of three parameters of the theoretical fit of Drude model to the experimental reflectance data, was found to decrease systematically with an increasing oxygen flow rate. Accordingly, independent measurements of the electrical conductivity revealed its decrease as a function of oxygen flow rate. Transition from metallic conductivity typical for stoichiometric TiN to semiconducting properties apparent for oxygen-doped Ti(ON) indicated that for samples prepared by dc-pulsed reactive magnetron sputtering applied in this work, oxygen could be successfully incorporated into TiN lattice.

Acknowledgments

The authors are grateful to O. Heintz for help in XPS experiments and H. Czternastek for Drude fits. This work was supported by the Polish Ministry of Education and Science (2008–2010) Grant no. N N507 458734.

References

[1] A. Mills, S. Le Hunte, J. Photochem. Photobiol. A 108 (1997) 1–35.
[2] M. Grätzel, Nature 414 (2001) 338–344.
[3] A.V. Emeline, V.N. Kuznetsov, V.K. Rybchuk, N. Serpone, Int. J. Photoenergy (2008), doi:10.1155/2008/258394.
[4] M. Radecka, M. Rekas, A. Trenczek-Zajac, K. Zakrzewska, J. Power Sources 181 (2008) 46–55.
[5] M.R. Hoffman, S.T. Martin, W. Choi, D.W. Bahnemann, Chem. Rev. 95 (1995) 69–96.
[6] H.P. Maruska, A.K. Gosh, Sol. Energy Mater. 1 (1979) 237–247.
[7] M. Radecka, M. Wierzbicka, S. Komornicki, M. Rekas, Physica B 348 (2004) 160–168.
[8] M. Radecka, K. Zakrzewska, M. Wierzbicka, A. Gorzkowska, S. Komornicki, Solid State Ionics 157 (2003) 379–386.
[9] K. Zakrzewska, M. Radecka, A. Kruk, W. Osuch, Solid State Ionics 157 (2003) 349–356.
[10] G. Zhao, H. Kozuka, H. Lin, T. Yoko, Thin Solid Films 339 (1999) 123–128.
[11] R. Asahi, T. Morikawa, T. Ohwaki, K. Aoki, Y. Taga, Science 293 (2001) 269–271.
[12] S.U.M. Khan, M. Al-Shahry, W.B. Ingler Jr., Science 297 (2002) 2243–2245.
[13] T. Umebayashi, T. Yamaki, H. Itoh, K. Asai, Appl. Phys. Lett. 81/3 (2002) 454–456.
[14] H. Irie, S. Washizuka, Y. Watanabe, T. Kako, K. Hashimotoz, J. Electrochem. Soc. 152/11 (2005) E351–E356.
[15] H. Wang, J.P. Lewis, J. Phys.: Condens. Matter 18 (2006) 421–434.
[16] C. Di Valentin, G.-F. Pacchioni, A. Selloni, Phys. Rev. B: Condens. Matter 70/8 (2004), Article ID 085116.
[17] F.-H. Lu, H.-Y. Chen, Thin Solid Films 355–356 (1999) 374–379.
[18] A. Brudnik, M. Bucko, M. Radecka, A. Trenczek-Zajac, K. Zakrzewska, Vacuum 32 (2008) 936–941.
[19] O. Diwald, T.L. Thompson, T. Zubkov, Ed.G. Goralski, S.D. Walck, J.T. Yates, J. Phys. Chem. B 108 (2004) 6004–6008.
[20] S.H. Mohamed, O. Kappertz, J.M. Ngaruiya, T. Niemeier, T.R. Drese, R. Detemple, M.M. Wakkad, M. Wutting, Phys. Stat. Sol. (a) 201 (2004) 90–102.
[21] T. Chiaramonte, L.P. Cardoso, R.V. Gelamo, F. Fabreguette, M. Sacilotti, M.C. Marco de Lucas, L. Imhoff, S. Bourgeois, Y. Kihn, M.-J. Casanove, Appl. Surf. Sci. 212–213 (2003) 661–666.
[22] F. Fabreguette, L. Imhoff, M. Maglione, B. Domenichini, M.C. Marco de Lucas, P. Sibilliot, S. Bourgeois, M. Sacilotti, Chem. Vap. Depos. 6 (2000) 109–114.
[23] F. Fabreguette, L. Imhoff, J. Guillot, B. Domenichini, M.C. Marco de Lucas, P. Sibilliot, S. Bourgeois, M. Sacilotti, Surf. Coat. Technol. 125 (2000) 396–399.
[24] J. Guillot, F. Fabreguette, L. Imhoff, O. Heintz, M.C. Marco de Lucas, M. Sacilotti, B. Domenichini, S. Bourgeois, Appl. Surf. Sci. 177 (2001) 268–272.
[25] J.M. Mwabora, T. Lindgren, E. Avendano, T.F. Jaramillo, J. Lu, S.-E. Lindquist, C.-G. Granqvist, J. Phys. Chem. B 108 (2004) 20193–20198.
[26] J. Guillot, J.-M. Chappé, O. Heintz, N. Martin, L. Imhoff, J. Takadoum, Acta Mater. 54 (2006) 3067–3074.

[27] F. Vaz, P. Cerqueira, L. Rebouta, S.M.C. Nascimento, E. Alves, Ph. Goudeau, J.P. Rivière, Surf. Coat. Technol. 174–175 (2003) 197–203.
[28] H.G. Tompkins, J. Appl. Phys. 71 (1992) 980–983.
[29] A. Brudnik, H. Czternastek, K. Zakrzewska, M. Jachimowski, Thin Solid Films 199/1 (1991) 45–58.
[30] W.M. Posadowski, A. Wiatrowski, J. Dora, Z.J. Radzimski, Thin Solid Films 516 (2008) 4478–4482.
[31] A. Trenczek-Zajac, M. Radecka, K. Zakrzewska, A. Brudnik, E. Kusior, S. Bourgeois, M.C. Marco de Lucas, L. Imhoff, Ann. Chim.: Sci. Mater. 33 (Suppl. 1) (2008) 149–156.
[32] P. Scherrer, Gott. Nachr. 2 (1918) 98–100.
[33] J.A. Thornton, J. Vac. Sci. Technol. A 4/6 (1986) 3059–3065.
[34] N. Schönberg, Acta Chem. Scand. 8 (1954) 208–212.
[35] J.-M. Chappe, N. Martin, J. Lintymer, F. Sthal, G. Terwagne, J. Takadoum, Appl. Surf. Sci. 253 (2007) 5312–5316.
[36] R.D. Shannon, Acta Cryst. A32 (1976) 751–767.
[37] J. Guillot, A. Jouaiti, L. Imhoff, B. Domenichini, O. Heintz, S. Zerkout, A. Mosser, S. Bourgeois, Surf. Interface Anal. 33 (2002) 577–582.
[38] No. 38-1420 of JCPDS-ICDD diffraction database PDF-2.
[39] No. 8-117 of JCPDS-ICDD diffraction database PDF-2.
[40] W. Sprengler, R. Kaiser, H. Bilz, Solid State Commun. 17 (1975) 19–22.
[41] S. Boukrouh, R. Bensaha, S. Bourgeois, E. Finot, M.C. Marco de Lucas, Thin Solid Films 516 (2008) 6353–6358.
[42] G.K. Mor, O.K. Varghese, M. Paulose, K. Shankar, C.A. Grimes, Sol. Energy Mater. Sol. Cells 90 (2006) 2011–2075.
[43] N.C. Saha, G.J. Tompkins, Appl. Phys. 72 (1992) 3072–3079.
[44] X. Song, D. Gopireddy, C.G. Takoudis, Thin Solid Films 516 (2008) 6330–6335.
[45] P. Xu, L. Mi, P.-N. Wang, J. Cryst. Growth 289 (2006) 433–439.
[46] Y. Li, G. Ma, S. Peng, G. Lu, S. Li, Appl. Surf. Sci. 254 (2008) 6831–6836.
[47] J. Yuan, M. Chen, J. Shi, W. Shangguan, Int. J. Hydrogen Energy 31/10 (2006) 1326–1331.
[48] B. Liu, X. Zhao, L. Wen, Surf. Coat. Technol. 201 (2006) 3606–3610.
[49] T. Aoki, K. Maki, Q. Tang, Y. Kumagai, S. Matsumoto, J. Vac. Sci. Technol. A 15/5 (1997) 2485–2488.
[50] T. Okato, T. Sakano, M. Obara, Phys. Rev. B: Condens. Matter 72 (2005) 115124.
[51] L. Wan, J.F. Li, J.Y. Feng, W. Sun, Z.Q. Mao, Appl. Surf. Sci. 253/10 (2007) 4764–4767.
[52] K.S. Robinson, P.M.A. Sherwood, Surf. Interface Anal. 6/6 (1984) 261–266.
[53] I. Bertoti, M. Mohai, J.L. Sullivan, S.O. Saied, Appl. Surf. Sci. 84 (1995) 357–371.
[54] I. Montero, C. Jimenez, J. Perriere, Surf. Sci. 251 (1991) 1038–1044.
[55] P. Prieto, R.E. Kirby, J. Vac. Sci. Technol. A 13 (1995) 2819–2826.
[56] F. Peng, L. Cai, L. Huang, H. Yu, H. Wang, J. Phys. Chem. Solids 69 (2008) 1657–1664.
[57] leR. Strydom, S. Hofmann, J. Electron. Spectrosc. Related Phenom. 56 (1991) 85–103.
[58] W.P. Dumke, Phys. Rev. 124/6 (1961) 1813–1817.
[59] H. Kostlin, R. Jost, W. Lems, Phys. Stat. Sol. (a) 29/1 (1975) 87–93.